Applied Thermal Engineering 200 (2022) 117674

Contents lists available at ScienceDirect

Applied Thermal Engineering

journal homepage: www.elsevier.com/locate/apthermeng

Design modification of two-dimensional supersonic ejector via the adjoint method

Hadi Samsam-Khayani [a], Seong Hyun Park [b], Man Yeong Ha [a], Kyung Chun Kim [a], Sang Youl Yoon [b,*]

[a] School of Mechanical Engineering, Pusan National University, Busan 46241, Republic of Korea
[b] Rolls-Royce and Pusan National University Technology Centre, Pusan National University, Busan 46241, Republic of Korea

ARTICLE INFO

Keywords:
Supersonic gas ejector
Adjoint method
Entrainment ratio
Compressible flow
Design modification

ABSTRACT

A numerical investigation of a design modification of a two-dimensional supersonic gas ejector was undertaken via an adjoint method, with a focus on enhancing the performance of the ejector. Maximization of the secondary mass flow rate was used as an objective function. The entrance geometry and throat height of the primary nozzle were fixed, but the other geometries were allowed to vary during the design modification. The shape of the divergence of the primary nozzle, the nozzle exit position (NXP), and the entrance region of the mixing chamber were modified simultaneously using the adjoint method. The height of divergent section of primary nozzle (H_{ne}), NXP, and the inlet height of the mixing chamber (H_{mi}) were enlarged by about 13.33%, 27%, and 49%, respectively, resulting in an entrainment ratio (ER) that was enhanced by about 37.17% compared to that obtained for the baseline geometry. Two simplified geometries from the adjoint modification were suggested, and have the same performance with the adjoint-modified geometry. Further investigation was performed by varying the height of the straight section of the mixing chamber of the simplified geometry. The results show that the ER increased by about 46.77% compared with that obtained using the simplified geometry.

1. Introduction

The twin benefits of ejectors, of having no moving parts and no restrictions on the working fluid, have led to their widespread use in various industrial and engineering fields, such as heat pumps in district heating systems [1], refrigeration systems [2–6], vacuum generators [7], fuel-cell recirculation systems [8], gas mixing [9], and noise suppression and thrust augmentation [10]. The productivity of all these systems is highly dependent upon the performance of the ejector. Specifically, the entrainment ratio (ER) is the ratio of secondary to primary mass flow rate, and can be affected by the operating conditions and geometrical parameters such as the diameter of the mixing chamber, the nozzle exit position (NXP), and the diameters of both the throat and the nozzle exit. CFD simulations have been used widely as an effective means of investigating the effects of these parameters on the performance of a supersonic ejector. For instance, conventional numerical approaches have been conducted to investigate effects of the cross-sectional area ratio of mixing chamber to primary nozzle throat [11], the suction chamber's angle [12], the nozzle exit position [12,13,14], the nozzle throat diameter and the mixing chamber diameter [14], and the length of the mixing chamber [15].

Fu et al. [16] showed that there is an optimum range of the ratio of the nozzle exit position to the throat of the primary nozzle, and an optimum range of the ratio of the throat of the mixing chamber to the throat of the primary nozzle, for which the ejector achieves its maximum performance. Sriveerakul et al. [17] investigated numerically the effect of operating pressures and various geometrical parameters on the performance of a steam ejector, and found that a small primary nozzle throat provided a high ER, although this meant that the ejector must be operated at a low back pressure. In contrast, they found that a large primary nozzle throat caused a large core jet with higher momentum, creating a smaller effective area and a lower ER as a result.

Yan et al. [18] also used a numerical approach, in their case to examine the modification of the design of an air-cooled ejector cooling system by considering six key parameters, namely the area ratio, NXP, the diverging angle of the nozzle, the converging angle of the mixing section, the length of the constant-area section, and the diffuser length.

* Corresponding author at: Rolls-Royce and Pusan National University Technology Centre, Pusan National University, 2, Busandaehak-ro 63beon-gil, Geumjeong-gu, Busan 46241, Republic of Korea.
E-mail address: yoonsy@pusan.ac.kr (S.Y. Yoon).

https://doi.org/10.1016/j.applthermaleng.2021.117674
Received 19 May 2021; Received in revised form 8 October 2021; Accepted 9 October 2021
Available online 13 October 2021

Nomenclature

English letter

ER	entrainment ratio (ER $= \dot{m}_s/\dot{m}_p$)
$\dot{m}$	mass flow rate [kg s^{-1}]
H	height [m]
L	length [m]
NXP	nozzle exit position [m]
x	coordinates

Greek letters

ρ	density [kg m^{-3}]
θ	angle [radian]

Subscripts

th	throat
p	primary flow
s	secondary flow
ne	nozzle exit
mi	mixing chamber inlet
ms	mixing chamber straight section
C	convergence section
m	mixing chamber
d	diffuser
div	divergence section
mp	mixing chamber peak

structure within the mixing chamber and the performance of the ejector, as well as describing the influence of the aerodynamic throat of the secondary flow on the performance of the ejector. They showed that by increasing the NXP and the converging angle of the mixing chamber, it was possible to enhance the ER by around 6% and 9%, respectively.

Conventional numerical parametric studies of the supersonic gas ejector designs require a significant investment in terms of computational resources and time. Furthermore, because the modification of the supersonic gas ejectors for enhanced performance involves a variety of design variables that are not independent, the process of modification is considered somewhat complex. The adjoint method could effectively calculate sensitivities of the objective function for a large number of design variables [20]. The adjoint method has been widely applied in various engineering fields such as aerodynamic [21–24] and thermal application [25–26] and so on. Reuther et al. [21] they showed that the optimization process of three-dimensional supersonic aircraft shape is dramatically accelerated by using the adjoint method. Day et al. [22] investigated capability of applying the adjoint method to aerodynamic optimization of vertical axis wind turbines (VAWT) blade, to minimize the unsteady flow effects. Elsayed [23] used discrete adjoint method for design modification of cylindrical gas cyclone vortex finder to minimize the pressure drop. Liu et al. [24] obtained a desirable thermal environment design for an airliner cabin by utilization of the adjoint method. Sun et al. [25] investigated optimization of three-dimensional heat sink for liquid cooling by using the adjoint method in order to minimize the average temperature on the heat source surface. Czerwinski et al. [26] utilized adjoint method to optimize geometrical shape of heat sink used for an electronic component cooling in a confined space.

The aim of the present study was to apply the adjoint method to the modification of a two-dimensional supersonic gas ejector design in terms of the influence of a few key elements: the divergence shape of the primary nozzle, the entrance region of the mixing chamber, and NXP. In this study, the maximization of the secondary mass flow rate has been selected as the objective function for the adjoint analysis. The distribution of the Mach number, the numerical schlieren visualization, and the distribution of the wall pressure in the mixing chamber were all compared in order to assess the effect of geometrical parameters on the performance of the ejector.

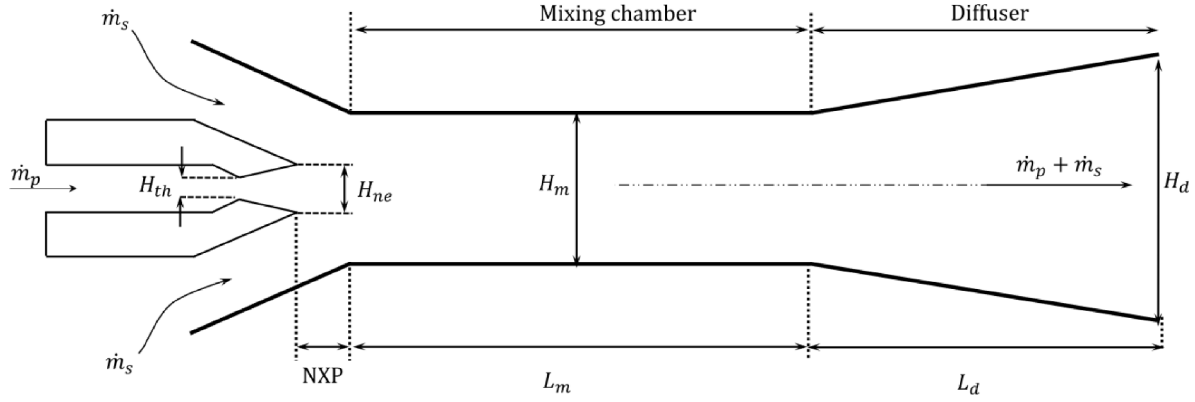

Fig. 1. Schematic diagram of a two-dimensional ejector showing the baseline geometry [27].

Table 1
Dimensions of the baseline geometry and boundary conditions [27].

Dimensions for baseline geometry				Boundary conditions	
Symbol	Size [mm]	Symbol	Size [mm]	Inlet/Outlet	Pressure [barg]
H_{th}	1.2	NXP	6	Primary inlet	6
H_{ne}	1.6	L_m	45	Secondary inlet	1
H_m	4	L_d	60	Outlet	2
H_d	12				

They used the optimized ejector to experimentally verify their numerical results. They presented that their findings highlighted a clear need to modify geometrical parameters such as the area ratio and NXP, both of which affect the performance of the ejector considerably.

Using a numerical approach, Metin et al. [19] considered the effect of NXP and the converging angle of the mixing chamber on both the flow

2. Numerical method

2.1. Physical model and boundary conditions

The general scheme of a two-dimensional ejector is shown in Fig. 1, which illustrates the baseline geometry used in this study. The ejector has four parts as follows: (i) primary nozzle, (ii) suction chamber, (iii) mixing chamber, and (iv) diffuser. The major dimensions (H_{th}, H_{ne}, H_m,

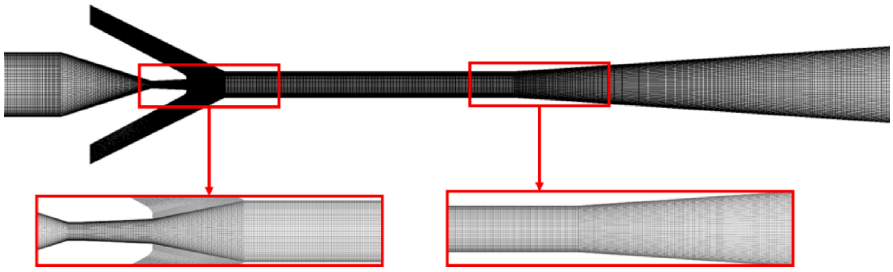

Fig. 2. Grids of the baseline geometry.

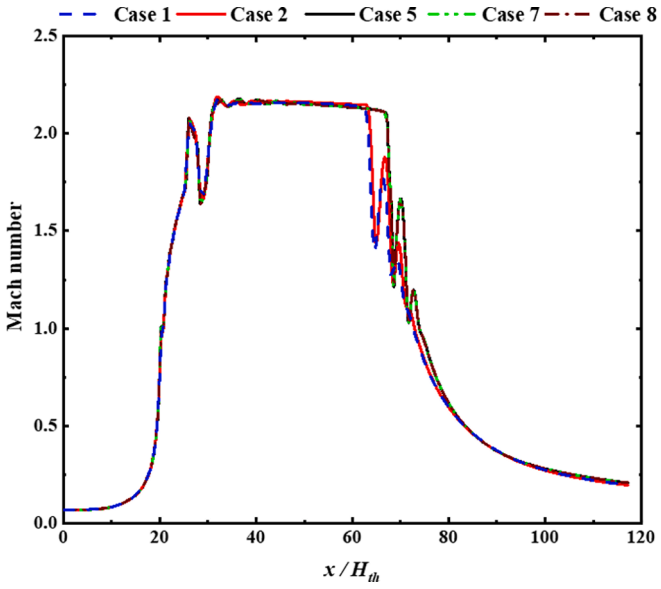

Fig. 3. Mach number distributions along the centerline for different mesh cases.

Table 2
Number of grid elements for each case.

Case	Number of elements	ER $_{present\ work}$
1	20,000	0.173
2	40,000	0.195
3	95,000	0.214
4	124,000	0.225
5	144,000	0.226
6	215,000	0.226
7	324,000	0.226
8	450,000	0.226

H_d, and NXP) of the ejector geometry were obtained from previous study [27]. The boundary conditions were determined with consideration of boundary conditions and results provided by Arun et al. [27]. The dimensions and boundary conditions are summarized in Table 1.

In the numerical simulations, the geometry of the ejector was considered two-dimensional, and the boundary conditions at the inlets (both the primary and secondary flows) and outlet are respectively defined as pressure-inlet and pressure-outlet, as shown in Table 1. Temperature boundary conditions for inlets and outlet were set as 300 K. In addition, a no-slip thermal insulation boundary condition was applied to the wall of the ejector. This geometry is termed the baseline geometry in all further investigations including the parametric study and the adjoint method.

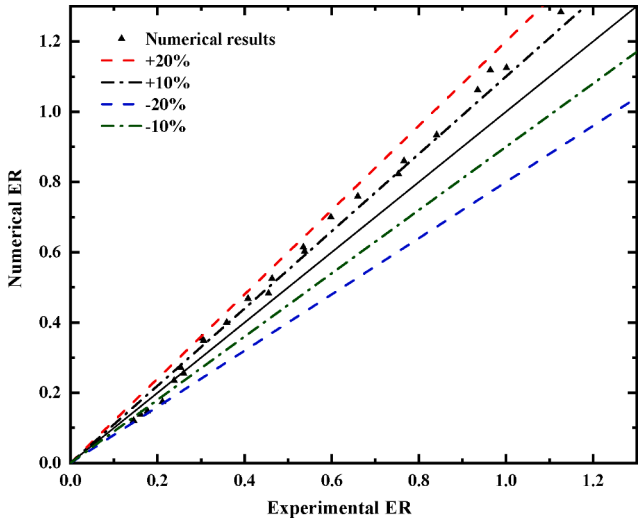

Fig. 4. Comparison of ER between experimental data by S.K. Karthick [34] and present numerical results.

2.2. Details of numerical method and validation

Numerical simulations were performed using the commercial software Ansys-Fluent v18.2. The compressible steady-state turbulent form of the flow and the heat transfer conservation equations were used to investigate the flow within the ejector. To simulate supersonic compressible flow, a density-based solver was used, similar to previous numerical simulations of supersonic ejectors [28]. The previous studies has reported the advantages of each turbulence model [29,30]. Numerical results using Realizable k-epsilon turbulent model showed good agreement with experimental data [30–32]. In the current study, Realizable k-epsilon turbulent model has been utilized.

The adjoint solver in Ansys Fluent has been applied to the finite volume solver by using the discrete approach, and can acquire sensitivities of the objective function for a large number of design variables via a single adjoint computation [33]. The detailed mathematical model and equations were discussed in Ref. [33]. For the adjoint investigation, in the design domain, the entrance geometry and throat height of the primary nozzle were fixed, whereas other geometries including those of the divergent section of the primary nozzle, the inlet region of the secondary flow, the mixing chamber, and the diffuser were allowed to vary.

With air as the working fluid, the ideal gas law was used for the density. Sutherland's law was used to obtain relationship between dynamic viscosity, μ, and the absolute temperature, T. Thermal conductivity was set to be constant value of 0.0242 [W/m.k]. For convergence, the accuracy of each residual must be less than 10^{-6}. Due to the complexity of the flow in a supersonic gas ejector, Full Multigrid initialization (FMG initialization) was used to accelerate the flow convergence and reach a better initial solution at the start of the calculation.

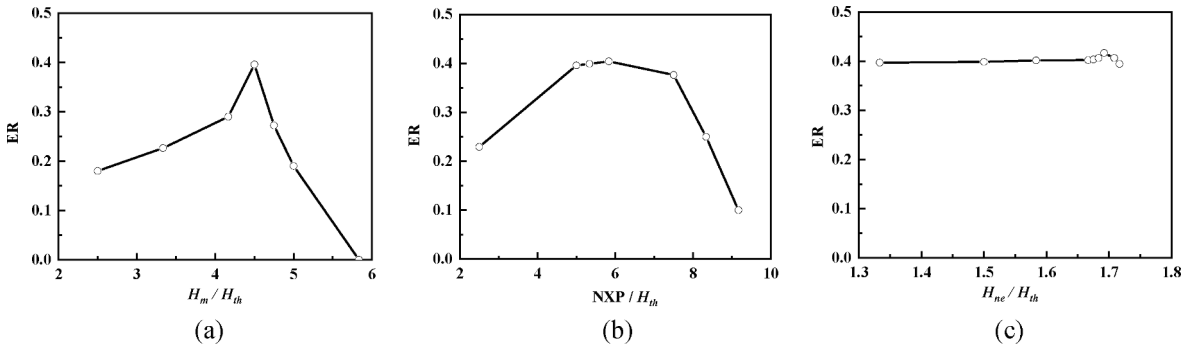

Fig. 5. Effect of geometrical parameters on ER; (a) H_m/H_{th} (b) NXP/H_{th} and (c) H_{ne}/H_{th}.

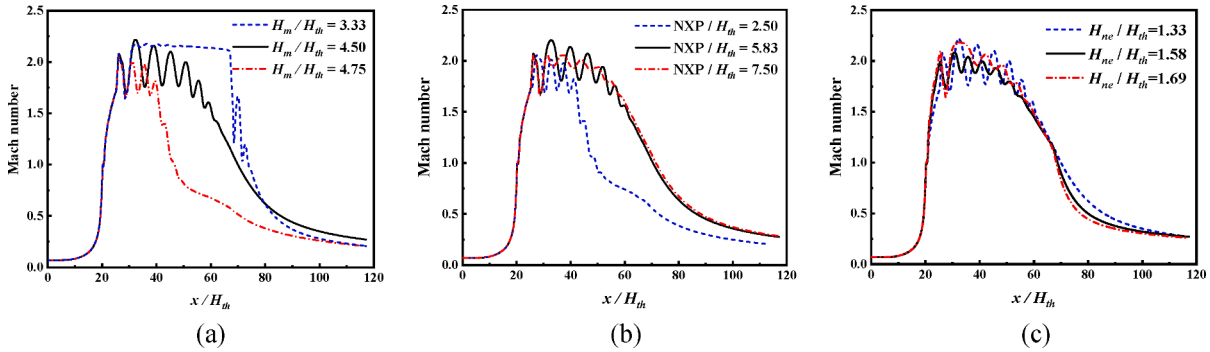

Fig. 6. Distributions of Mach number along centerline; (a) H_m/H_{th} (b) NXP/H_{th} and (c) H_{ne}/H_{th}.

A piecewise polynomial as a function of temperature was utilized for the specific heat of the fluid. A second-order upwind and a central difference scheme were applied to discretize the advection and diffusion terms of the governing equations, respectively.

A grid dependency test was carried out using the baseline geometry and the boundary conditions considered in the present study. Quadrilateral structured grids were considered in order to allow better convergence of the solution (Fig. 2). Eight different sizes of grid were considered, ranging from a coarse (20000 elements) to a fine grid system (450000 elements). Fig. 3 and Table 2 show the results of the grid dependency test and Mach number distribution along the centerline and entrainment ratio, respectively. Results revealed a negligible difference when the number of elements exceeded 144000. A grid system with 144,000 elements was therefore deemed sufficient for this study.

Validation investigation have been performed using the experimental results reported by S.K. Karthick et al. [34]. As shown in Fig. 4, the present numerical simulation results showed good agreement with experimental data reported by S.K. Karthick et al. [34] (Minimum and maximum relative difference between numerical simulation and experimental results are −1.42% and −17.34%, respectively).

3. Results and discussion of shape modification

3.1. Parametric study based on baseline design

A conventional parametric study based on the baseline geometry was carried out to investigate the design modification of geometrical parameters including H_m, H_{ne}, and NXP. The boundary conditions for the inlets and outlet were fixed according to the values given in Table 1.

The effects of geometrical parameters on ER, the distribution of Mach number along the centerline, and the Mach number contours for H_m, H_{ne}, and NXP are shown in Figs. 5, 6, and 7, respectively. Fig. 5(a) shows that increasing the height of the mixing chamber up to H_m/H_{th} = 4.50 causes an increase of ER due to the enlargement of the effective area. Further enlargement of H_m leads to a decreasing ER caused by the reduced effect of the shear mixing layer between the primary and secondary flow. Fig. 6(a) and Fig. 7(a–c) show that the shock waves are stronger for $H_m/H_{th} = 4.50$ than for the other cases. The asymmetric flow in diffuser section were observed at some cases in Fig. 7. While the shock waves were formed within the diffuser part, the interaction between shock waves and corner boundary layer leads to a flow asymmetric at the downstream of shock waves [27,35,36].

As shown in Fig. 5(b), ER increased with NXP up to NXP/$H_{th} = 5.83$, but further increases in NXP led to a decrease in ER as the effective area of secondary flow and shear mixing layer decreased. Fig. 6(b) and Fig. 7 (d–f) show a decreased entrainment ratio caused by weaker shock waves. The variation in ER for different primary nozzle exit heights is shown in Fig. 5(c), in which it is clear that increasing H_{ne} of the primary nozzle caused a slightly enhanced ER up to $H_{ne}/H_{th} = 1.69$. Fig. 6(c) and Fig. 7(g–i) also show no significant difference in the shock waves for different values of H_{ne}.

3.2. Applying the adjoint method to the baseline ejector design.

As mentioned in Section 2.2, the adjoint method could be used to handle various geometrical parameters simultaneously, hence it was applied to the supersonic gas ejector to assess the ability of this method to modify the key parameters H_{ne}, NXP, and H_m. After calculating the flow field for the baseline geometry, the adjoint method is applied to calculate the sensitivities of the objective function, and modified the geometry and mesh, subsequently. Then, the flow field for the adjoint-modified geometry is computed. Fig. 8 presents a flowchart of the

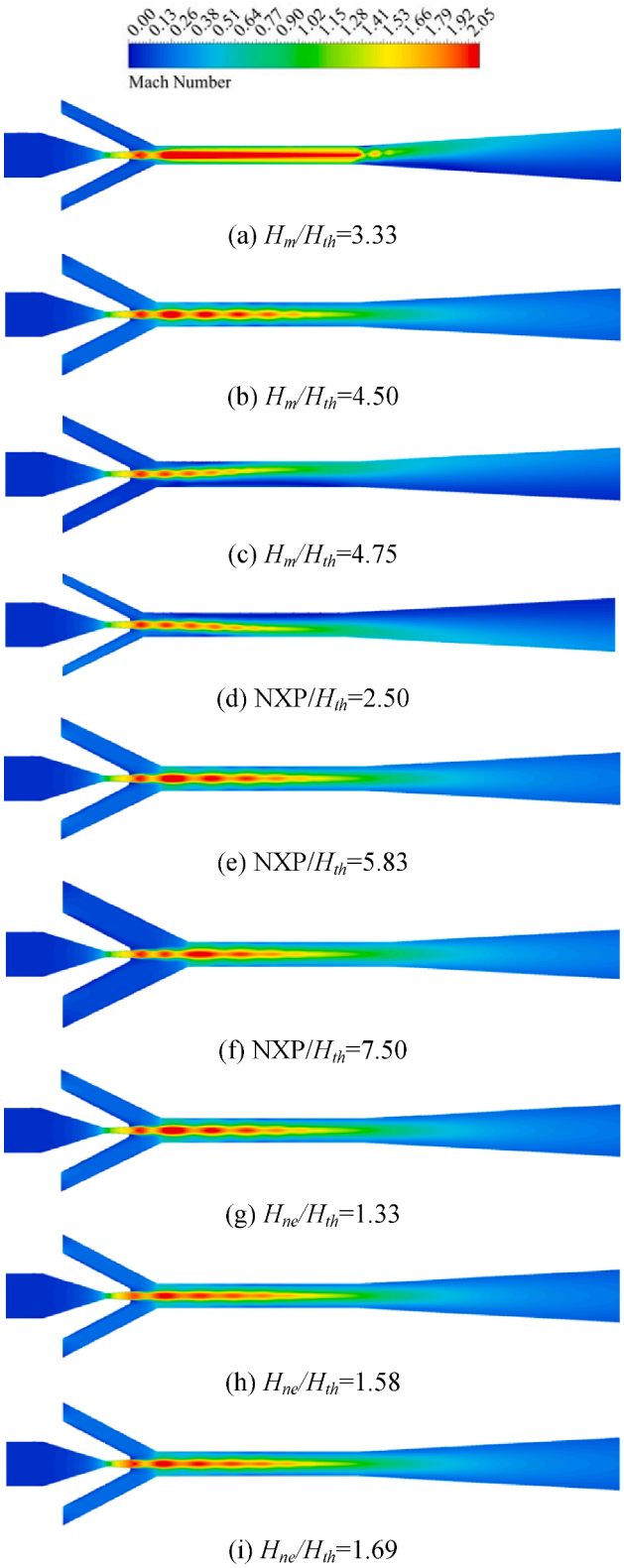

Fig. 7. Mach number contours for the geometrical parameters; (a-c) H_m/H_{th}, (d-f) NXP/H_{th} and (g-i) H_{ne}/H_{th}.

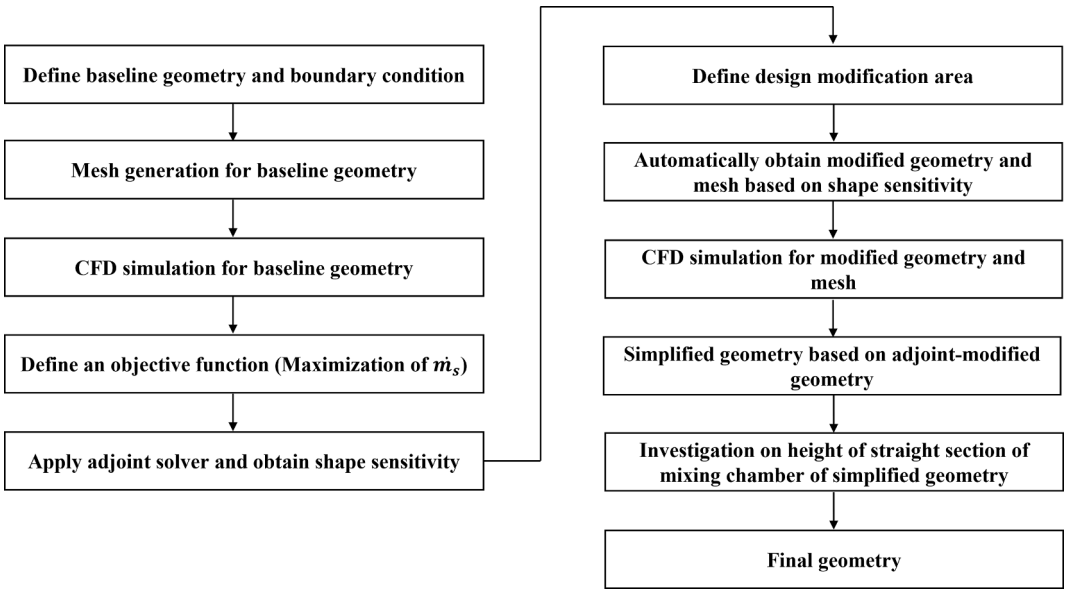

Fig. 8. Flowchart of the design modification process in this study.

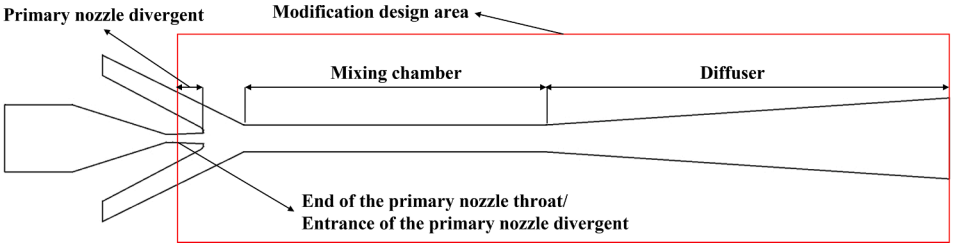

Fig. 9. Design modification area.

design modification process in this study.

In this study, in the design domain, the primary nozzle's entrance geometry and throat height are fixed, but the other sections, i.e., divergence section of the primary nozzle, NXP, mixing chamber, and diffuser, are allowed to vary during the design modification. Fig. 9 illustrates the design modification area defined in this study. The area is ranged from the entrance of divergence section of primary nozzle to the end of diffuser part. Since the fixed primary nozzle throat leads to the fixed primary mass flow rate, maximization of the secondary mass flow rate is set as the objective function to enhance the performance of the supersonic ejector. The adjoint calculation was fully converged after 135 iterations. The residuals for adjoint continuity, adjoint x-velocity, adjoint y-velocity, adjoint local flow rate, and adjoint energy were reached to in the order of 10^{-11}, 10^{-14}, 10^{-14}, 10^{-16}, and 10^{-10}, respectively.

The results of the adjoint method are compared to those for the baseline geometry as shown in Figs. 10–13. Figs. 10–11 show the Mach number contours and numerical schlieren visualization (density gradient; $\partial\rho/\partial y$). These figures indicate that three sections were modified simultaneously: the entrance region of the mixing chamber, NXP, and H_{ne}. Figs. 10 and 11 show that entrance region of the mixing chamber, NXP, and H_{ne} are enlarged compared with the baseline geometry, which could cause an increase of the effective area. In addition, as shown in Figs. 10 and 11, the primary jet flow changed from under-expanded (baseline geometry) to over-expanded (modified geometry via adjoint method) due to the enlarged divergence section of the primary nozzle. Fig. 12 shows a comparison of the distribution of Mach number along the centerline and the wall static pressure between the baseline and the modified geometry. According to Fig. 12(a), the modified geometry from the adjoint method shows stronger shock waves compared to the baseline geometry. Fig. 12(b) depicts the distribution of the wall static pressure at the convergent passage ahead of the mixing chamber, on the wall of the mixing chamber, and in the diffuser. It shows that the wall static pressure at the mixing chamber for the modified geometry is higher than that for the baseline geometry, which could allow better mixing of fluid in the mixing chamber [34]. Fig. 13 provides a more detailed comparison between the baseline geometry and the modified geometry from the adjoint method.

Table 3 provides a comparison of the three main design parameters and ER between the baseline and the modified geometry from the adjoint method. The exit height of the primary nozzle (H_{ne}), the nozzle exit position (NXP), and inlet height of the mixing chamber (H_{mi}), were increased by about 27%, 13%, and 49% from the baseline, respectively. The increase in NXP means that the length of the mixing chamber decreases by about $L_{m,\text{adjoint}}/L_{m,\text{baseline}} = 0.977$. The ER for the baseline geometry is 0.226 and for the modified geometry it is 0.310, showing an improvement of about 37.17% using the adjoint method.

3.3. Design modification based on the adjoint results

The modified geometry from the adjoint method (Fig. 13) contained walls that were curved arbitrarily, which would make the manufacturing process rather difficult; therefore, based on the adjoint recommendations two possible simplified geometries were investigated as shown in Fig. 14. For Case 1 with a distance of $\Delta L_1/L_m = 0.0393$, the height of the mixing chamber was enlarged to give $H_m/H_{th} = 5.167$, which then reduced to a straight section at $\Delta L_2/L_m = 0.44$, thus resembling the modified geometry via the adjoint method. For Case 2 a simpler geometry was used, with a convergent-straight section as shown in Fig. 14. The Mach number contours for these two geometries are

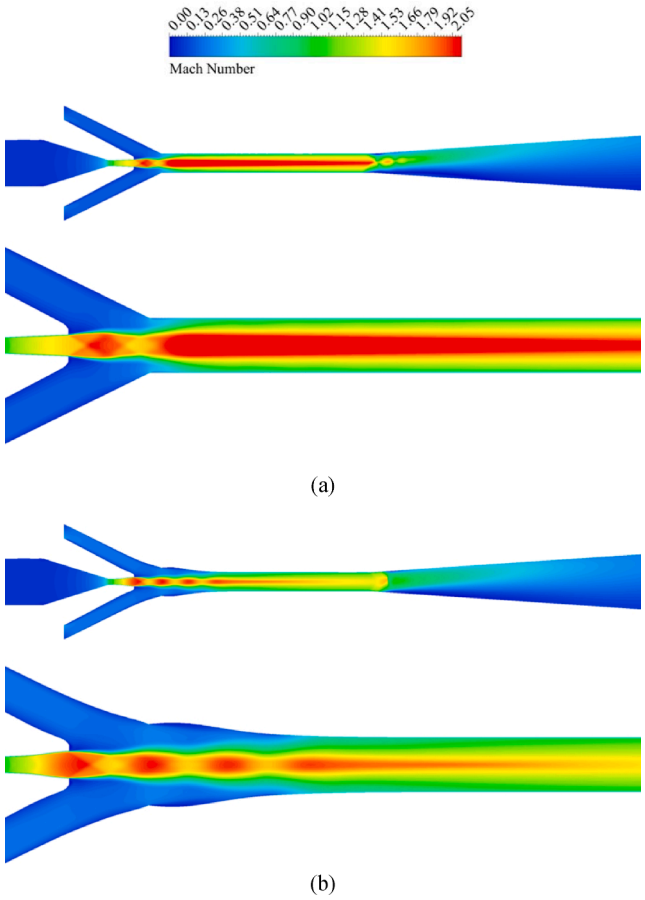

Fig. 10. Mach number contours of full domain and entrance region: (a) the baseline geometry, (b) the modified geometry via the adjoint method.

shown in Fig. 15, and these are similar to the adjoint results in Section 3.2. The ERs for these two cases are around 0.310, in good agreement with the results of the adjoint method. We considered Case 2 for further investigation due to its simpler geometry compared with Case 1.

3.3.1. *Investigation of the adjoint recommendations*

An analysis of the convergent section of the mixing chamber and the divergent section of the primary nozzle for the Case 2 geometry was performed in order to assess the capability of the adjoint method for design modification of a supersonic gas ejector. The investigation was conducted with various values of H_{ne}, H_{mi}, and L_C with the Case 2 geometry.

The distributions of Mach number for various H_{ne}, H_{mi}, and L_C are shown in Figs. 16 and 17. The variation of ER with varying H_{ne}, H_{mi}, and L_C are summarized in Table 4. Table 4 shows that ER reached to its maximum value of 0.310 when $H_{ne}/H_{th} = 1.69$, $H_{mi}/H_{th} = 4.97$, and $L_c/L_m = 0.44$ which were recommended by the adjoint method in Section 3.2. This investigation reveals that the adjoint method could provide a modified geometry in the divergent section of the primary nozzle and the entrance region of the mixing chamber with enhanced performance of an ejector.

3.3.2. *Further modification of the mixing chamber*

In the previous section, we showed that the adjoint method can be used to modify appropriately the primary nozzle shape, NXP, and the entrance region of the mixing chamber. However, as shown in Fig. 13, the adjoint method cannot be used to modify the whole geometry of the mixing chamber; hence it was necessary to investigate the effect of the height of the straight section of the mixing chamber (H_{ms}) on ER. Figs. 18 and 19 present the distributions of Mach number. The ERs for various values of H_{ms} are listed in Table 5.

Figs. 18 and 19 show that by increasing the height of the straight section of the mixing chamber up to $H_{ms}/H_{th} = 4.50$, the shock waves become stronger. As shown in Table 5, the ER increased to 0.455 when $H_{ms}/H_{th} = 4.50$. While the adjoint method allowed ER to increase from 0.226 (baseline geometry) to 0.310, it was increased further to around 0.455 following modification of the straight section of the mixing chamber.

4. Conclusions

The present findings show that the adjoint method can be used to modify the design of a two-dimensional supersonic gas ejector by focusing on the enhancement of the entrainment ratio (ER). The secondary mass flow rate was maximized, and this was considered to be the objective function for enhancing ER. In the current approach the adjoint method has been applied while the boundary conditions are fixed.

The primary nozzle shape, the nozzle exit position (NXP), and the shape of the entrance of the mixing chamber were modified simultaneously by using the adjoint method. Through the modification, three key geometrical parameters including exit height of the primary nozzle (H_{ne}), NXP, and inlet height of the mixing chamber (H_{mi}), were increased by about 27%, 13%, and 49% from the baseline geometry, respectively. Then, the effective area was enlarged, and this caused ER to increase. Consequently, the adjoint method was used to increase ER by around 37.17% (ER = 0.310 for the modified geometry via the adjoint method; ER = 0.226 for the baseline geometry) compared to that obtained for the baseline geometry. Two simplified geometries, Case 1 and 2, based on the adjoint-modified geometry were suggested, and produced same performance as the adjoint result. In order to assess the design

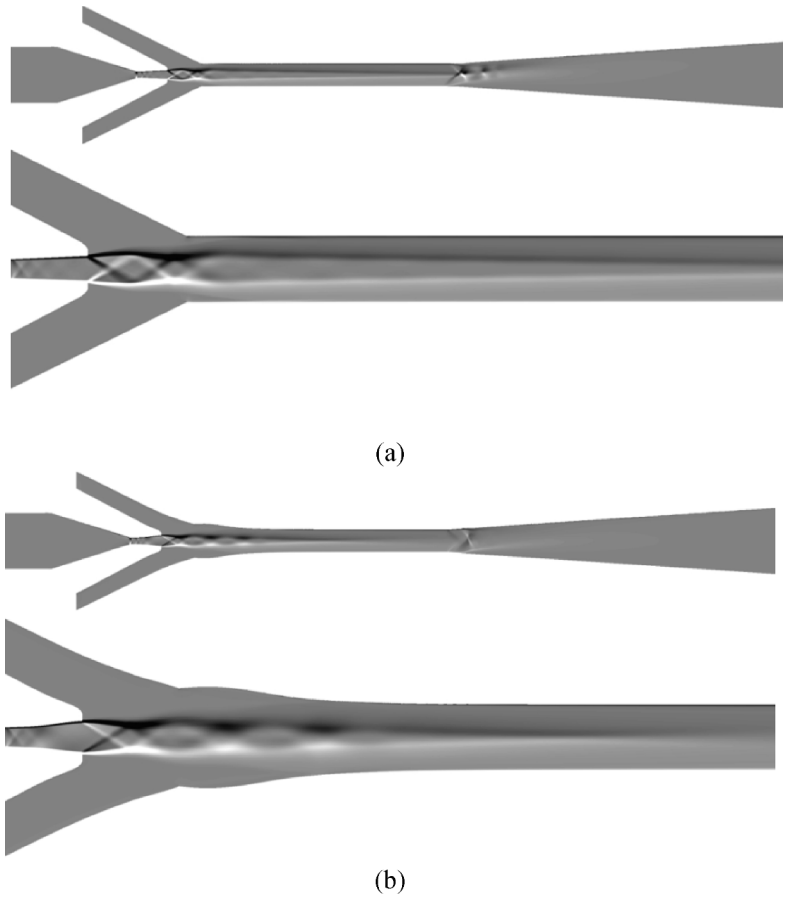

Fig. 11. Numerical schlieren visualization of full domain and entrance region ($\partial\rho/\partial y$): (a) the baseline geometry, (b) the modified geometry from the adjoint method.

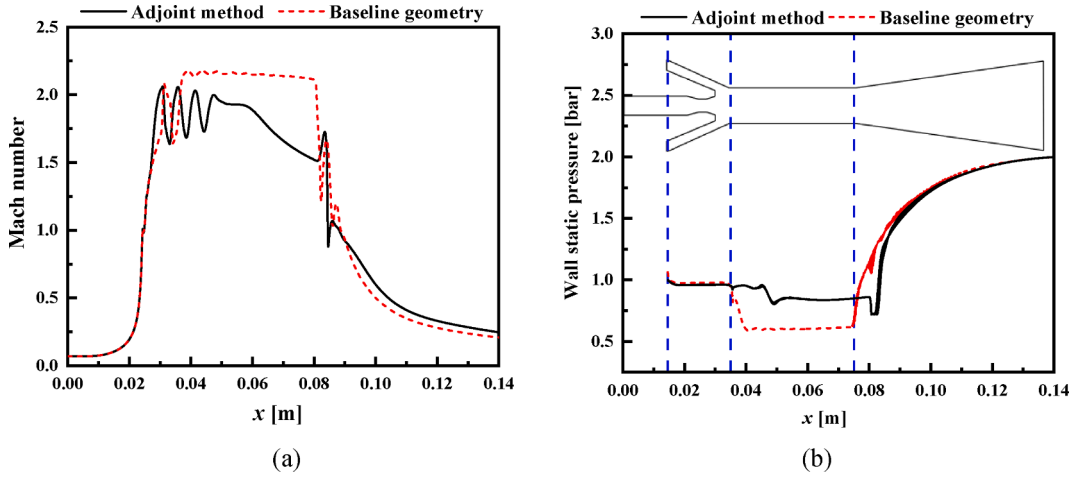

Fig. 12. Comparison of (a) Mach number distribution along the centerline and (b) wall static pressure profile; for the baseline geometry and the modified geometry via the adjoint method.

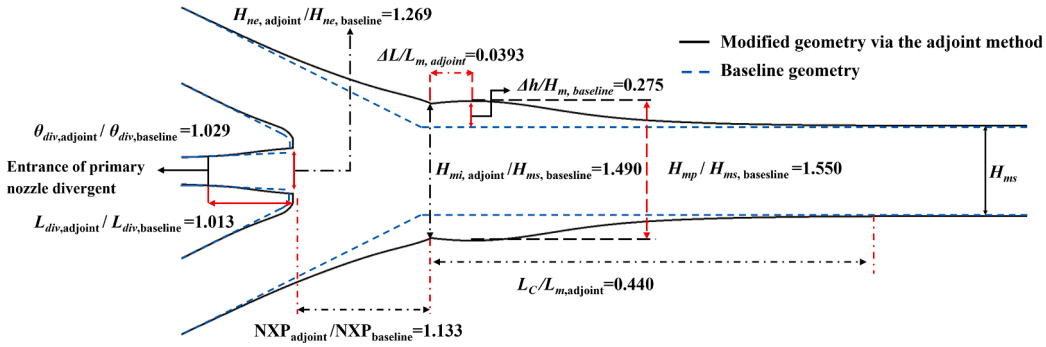

Fig. 13. Comparison between the baseline geometry and the modified geometry via the adjoint method.

Table 3
Main design parameters and ER for the baseline and adjoint-modified geometry.

Case	H_{ne}/H_{th}	NXP/H_{th}	H_{mi}/H_{th}	Mass flow rate [kg/s]		ER	Increase (%)
				Primary	Secondary		
Baseline geometry	1.33	5.00	3.33	1.6517	0.3734	0.226	–
Adjoint-modified geometry	1.69	5.60	4.97	1.6517	0.5123	0.310	37.17

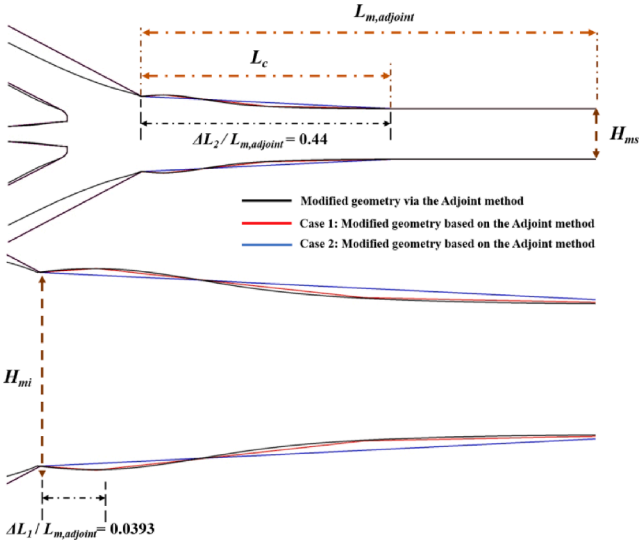

Fig. 14. Modified mixing chamber's shape for the two simplified modified geometries based on the adjoint method.

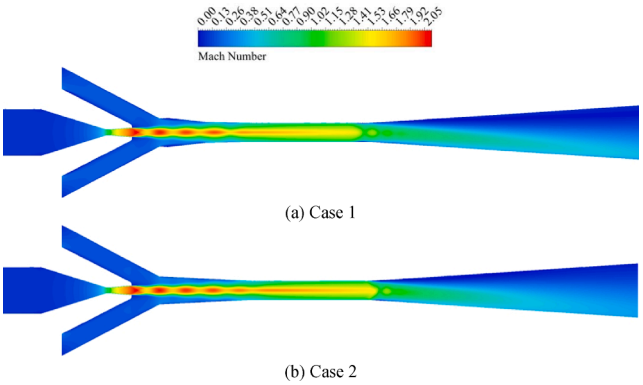

Fig. 15. Mach number contours for the two simplified modified geometries based on the adjoint method.

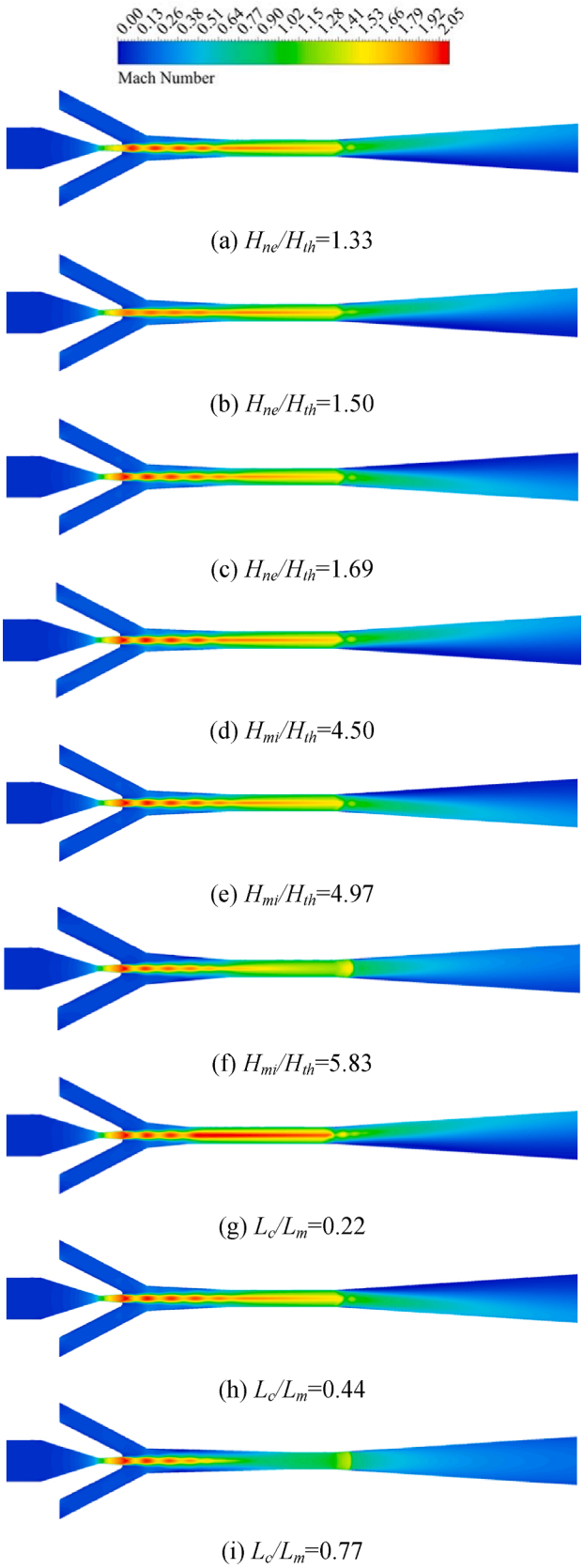

Fig. 16. Mach number contours with varying H_{ne}, H_{mi}, and L_c of Case 2 geometry; (c), (e), and (h) are for the case 2 geometry.

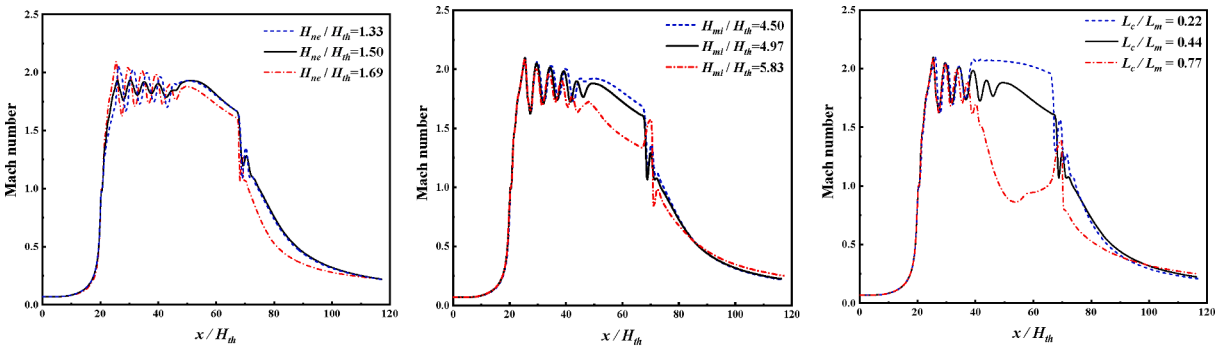

Fig. 17. Distributions of Mach number along the centerline with varying H_{ne}, H_{mi}, and L_c of Case 2 geometry.

Table 4
Entrainment ratio with varying H_{ne}, H_{mi}, and L_c of Case 2 simplified geometry.

Modification case	H_{ne}/H_{th}	H_{mi}/H_{th}	L_C/L_m	H_{ms}/H_{th}	ER	Remark
H_{ne}	1.33	4.97	0.44	3.33	0.285	–
	1.50				0.296	–
	1.58				0.299	–
	1.67				0.300	–
	1.69				0.310	Adjoint recommendation
	1.80				0.308	–
	1.90				0.300	–
H_{mi}	1.69	4.50	0.44	3.33	0.298	
		4.97			0.310	Adjoint recommendation
		5.17			0.293	–
		5.83			0.284	–
		6.25			0.271	–
L_C	1.69	4.97	0.22	3.33	0.261	–
			0.33		0.283	–
			0.44		0.310	Adjoint recommendation
			0.55		0.306	–
			0.77		0.302	–

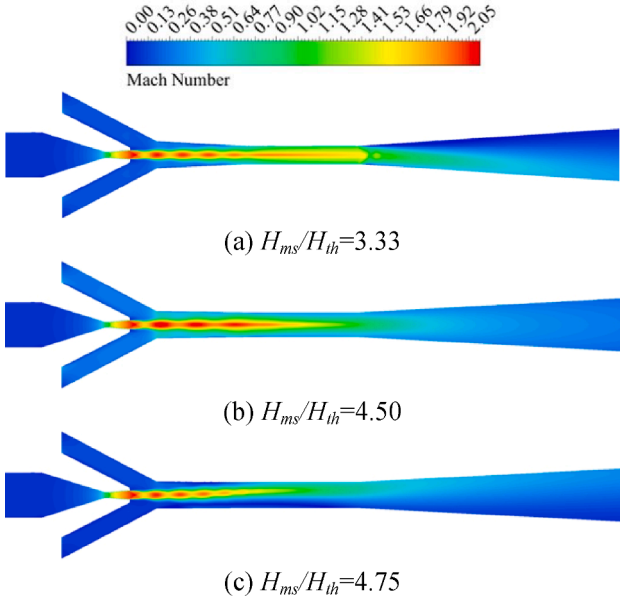

Fig. 18. Mach number contours for H_{ms}/H_{th} = 3.33, 4.50, and 4.75.

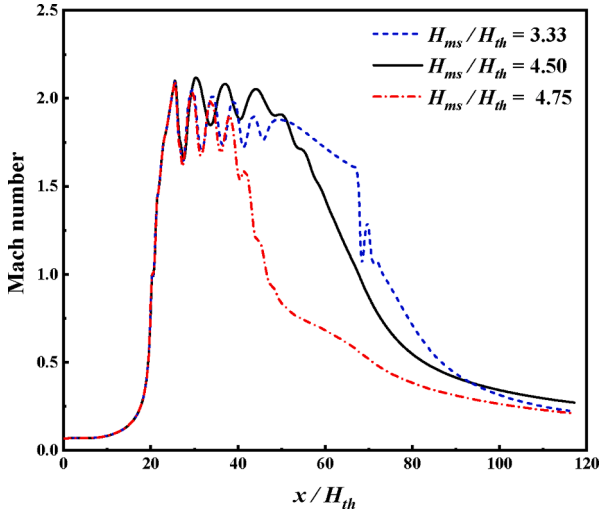

Fig. 19. Distributions of Mach number along the centerline for H_{ms}/H_{th} = 3.33, 4.50, and 4.75.

Table 5
Entrainment ratio for various height of the straight section of the mixing chamber.

H_{ne}/H_{th}	H_{mi}/H_{th}	L_C/L_m	H_{ms}/H_{th}	ER
1.69	4.97	0.44	2.91	0.254
			3.33	0.301
			4.17	0.408
			4.33	0.442
			4.50	0.455
			4.75	0.209

modification via the adjoint method, numerical investigation with varying H_{ne}, H_{mi}, and L_c of Case 2 simplified geometry was conducted, and the results showed that the adjoint method properly modified the divergent section of the primary nozzle and convergent section of mixing chamber. In addition, investigations were undertaken in which the height of the mixing chamber (H_{ms}) in the straight section was varied compared with the simplified geometry (Case2), revealing the possibility of increasing ER up to 0.455.

Declaration of Competing Interest

The authors declare that they have no known competing financial interests or personal relationships that could have appeared to influence the work reported in this paper.

Acknowledgement

This research was supported by Basic Science Research Program through the National Research Foundation of Korea(NRF) funded by the Ministry of Education(NRF-2018R1D1A1B07049379).

References

[1] B. Zhang, Y. Wang, L. Kang, J. Lv, Study of an innovative ejector heat pump-boosted district heating system, Appl. Therm. Eng. 58 (2013) 98–107, https://doi.org/10.1016/j.applthermaleng.2013.04.021.
[2] C. Lin, W. Cai, Y. Li, J. Yan, Y. Hu, Pressure recovery ratio in a variable cooling loads ejector-based multi-evaporator refrigeration system, Energy. 44 (2012) 649–656, https://doi.org/10.1016/j.energy.2012.05.027.
[3] N. Ruangtrakoon, S. Aphornratana, Design of steam ejector in a refrigeration application based on thermodynamic performance analysis, Sustain. Energy Technol. Assessments. 31 (2019) 369–382, https://doi.org/10.1016/j.seta.2018.12.014.
[4] Y. Li, J. Yu, The effects of ejector geometry parameter and refrigerant charge amount on an ejector-expansion refrigeration system, Appl. Therm. Eng. 152 (2019) 402–408, https://doi.org/10.1016/j.applthermaleng.2019.02.078.
[5] G. Besagni, R. Mereu, F. Inzoli, Ejector refrigeration: A comprehensive review, Renew. Sustain. Energy Rev. 53 (2016) 373–407, https://doi.org/10.1016/j.rser.2015.08.059.
[6] X. Wang, L. Wang, Y. Song, J. Deng, Y. Zhan, Optimal design of two-stage ejector for subzero refrigeration system on fishing vessel, Appl. Therm. Eng. 187 (2021), 116565, https://doi.org/10.1016/j.applthermaleng.2021.116565.
[7] H. Xue, L. Wang, L. Jia, C. Xie, Q. Lv, Design and investigation of a two-stage vacuum ejector for MED-TVC system, Appl. Therm. Eng. 167 (2020), 114713, https://doi.org/10.1016/j.applthermaleng.2021.117302.
[8] Z. Hailun, W. Sun, H. Xue, W. Sun, L. Wang, L. Jia, Performance analysis and prediction of ejector-based hydrogen recycle system under variable proton exchange membrane fuel cell working conditions, Appl. Therm. Eng. 197 (2021), 117302, https://doi.org/10.1016/j.applthermaleng.2021.117302.
[9] W. Ye, J. Zhang, W. Xu, Z. Zhang, Numerical investigation on the flow structures of the multi-strut mixing enhancement ejector, Appl. Therm. Eng. 179 (2020), 115653, https://doi.org/10.1016/j.applthermaleng.2020.115653.
[10] G. Raman, R. Taghavi, Aeroacoustic characteristics of a rectangular multi-element supersonic jet mixer-ejector nozzle, J. Sound Vib. 207 (1997) 227–248, https://doi.org/10.1006/jsvi.1997.1100.
[11] W. Gu, X. Wang, L. Wang, X. Yin, H. Liu, Performance investigation of an auto-tuning area ratio ejector for MED-TVC desalination system, Appl. Therm. Eng. 155 (2019) 470–479, https://doi.org/10.1016/j.applthermaleng.2019.04.018.
[12] A.S. Ramesh, S.J. Sekhar, Experimental and numerical investigations on the effect of suction chamber angle and nozzle exit position of a steam-jet ejector, Energy. 164 (2018) 1097–1113, https://doi.org/10.1016/j.energy.2018.09.010.
[13] K. Zhang, X. Zhu, X. Ren, Q. Qiu, S. Shen, Numerical investigation on the effect of nozzle position for design of high performance ejector, Appl. Therm. Eng. 126 (2017) 594–601, https://doi.org/10.1016/j.applthermaleng.2017.07.085.
[14] A. Mohammadi, An investigation of geometrical factors of multi-stage steam ejectors for air suction, Energy. 186 (2019), 115808, https://doi.org/10.1016/j.energy.2019.07.138.
[15] J. Dong, Q. Hu, M. Yu, Z. Han, W. Cui, D. Liang, H. Ma, X. Pan, Numerical investigation on the influence of mixing chamber length on steam ejector performance, Appl. Therm. Eng. 174 (2020), 115204, https://doi.org/10.1016/j.applthermaleng.2020.115204.
[16] W. Fu, Z. Liu, Y. Li, H. Wu, Y. Tang, Numerical study for the influences of primary steam nozzle distance and mixing chamber throat diameter on steam ejector performance, Int. J. Therm. Sci. 132 (2018) 509–516, https://doi.org/10.1016/j.ijthermalsci.2018.06.033.
[17] T. Sriveerakul, S. Aphornratana, K. Chunnanond, Performance prediction of steam ejector using computational fluid dynamics: Part 2. Flow structure of a steam ejector influenced by operating pressures and geometries, Int. J. Therm. Sci. 46 (2007) 823–833, https://doi.org/10.1016/j.ijthermalsci.2006.10.012.
[18] J. Yan, W. Cai, Y. Li, Geometry parameters effect for air-cooled ejector cooling systems with R134a refrigerant, Renew. Energy. 46 (2012) 155–163, https://doi.org/10.1016/j.renene.2012.03.031.
[19] C. Metin, O. Gök, A.U. Atmaca, A. Erek, Numerical investigation of the flow structures inside mixing section of the ejector, Energy 166 (2019) 1216–1228, https://doi.org/10.1016/j.energy.2018.10.095.
[20] M.B. Giles, N.A. Pierce, An introduction to the adjoint approach to design, Flow, Turbul. Combust. 65 (2000) 393–415, https://doi.org/10.1023/A:1011430410075.
[21] J. Reuther, J.J. Alonso, M.J. Rimlinger, A. Jameson, Aerodynamic shape optimization of supersonic aircraft configurations via an adjoint formulation on distributed memory parallel computers, Comput. Fluids. 28 (1999) 675–700, https://doi.org/10.1016/S0045-7930(98)00050-4.
[22] H. Day, D. Ingham, L. Ma, M. Pourkashanian, Adjoint based optimisation for efficient VAWT blade aerodynamics using CFD, J. Wind Eng. Ind. Aerodyn. 208 (2021), 104431, https://doi.org/10.1016/j.jweia.2020.104431.
[23] K. Elsayed, Design of a novel gas cyclone vortex finder using the adjoint method, Sep. Purif. Technol. 142 (2015) 274–286, https://doi.org/10.1016/j.seppur.2015.01.010.
[24] W. Liu, R. Duan, C. Chen, C.H. Lin, Q. Chen, Inverse design of the thermal environment in an airliner cabin by use of the CFD-based adjoint method, Energy Build. 104 (2015) 147–155, https://doi.org/10.1016/j.enbuild.2015.07.011.
[25] S. Sun, P. Liebersbach, X. Qian, 3D topology optimization of heat sinks for liquid cooling, Appl. Therm. Eng. 178 (2020), 115540, https://doi.org/10.1016/j.applthermaleng.2020.115540.
[26] G. Czerwiński, J. Wołoszyn, Optimization of air-cooling system using adjoint solver technique, Energies 14 (2021), https://doi.org/10.3390/en14133753.
[27] K.M. Arun, S. Tiwari, A. Mani, Three-dimensional numerical investigations on rectangular cross-section ejector, Int. J. Therm. Sci. 122 (2017) 257–265, https://doi.org/10.1016/j.ijthermalsci.2017.08.024.
[28] G. Besagni, F. Inzoli, Computational fluid-dynamics modeling of supersonic ejectors: Screening of turbulence modeling approaches, Appl. Therm. Eng. 117 (2017) 122–144, https://doi.org/10.1016/j.applthermaleng.2017.02.011.
[29] G. Besagni, N. Cristiani, L. Croci, G.R. Guédon, F. Inzoli, Computational fluid-dynamics modelling of supersonic ejectors: Screening of modelling approaches, comprehensive validation and assessment of ejector component efficiencies, Appl. Therm. Eng. 186 (2021), https://doi.org/10.1016/j.applthermaleng.2020.116431.
[30] Y. Han, X. Wang, H. Sun, G. Zhang, L. Guo, J. Tu, CFD simulation on the boundary layer separation in the steam ejector and its influence on the pumping performance, Energy 167 (2019) 469–483, https://doi.org/10.1016/j.energy.2018.10.195.
[31] N. Ruangtrakoon, T. Thongtip, S. Aphornratana, T. Sriveerakul, CFD simulation on the effect of primary nozzle geometries for a steam ejector in refrigeration cycle, Int. J. Therm. Sci. 63 (2013) 133–145, https://doi.org/10.1016/j.ijthermalsci.2012.07.009.
[32] N. Sharifi, M. Boroomand, An investigation of thermo-compressor design by analysis and experiment: Part 1. Validation of the numerical method, Energy Convers. Manag. 69 (2013) 217–227, https://doi.org/10.1016/j.enconman.2012.12.009.
[33] ANSYS, ANSYS FLUENT Adjoint Solver, ANSYS, Inc., Southpointe, 275 Technology Drive, Canonsburg, PA 15317, USA, 2013.
[34] S.K. Karthick, S.M.V. Rao, G. Jagadeesh, K.P.J. Reddy, Parametric experimental studies on mixing characteristics within a low area ratio rectangular supersonic gaseous ejector, Phys. Fluids 28 (2016), https://doi.org/10.1063/1.4954669.
[35] M. Sajben, T.J. Bogar, J.C. Kroutil, Forced oscillation experiments in supercritical diffuser flows, AIAA J. 22 (1984) 465–474, https://doi.org/10.2514/3.8423.
[36] P.J.K. Bruce, H. Babinsky, B. Tartinville, C. Hirsch, Corner Effect and Asymmetry in Transonic Channel Flows, AIAA J. 49 (2011) 2382–2392, https://doi.org/10.2514/1.j050497.